ChemComm

Redox- and Light-Switchable N-Heterocyclic Carbenes: A "Soup-to-Nuts" Course on Contemporary Structure–Activity Relationships

Journal:	*ChemComm*
Manuscript ID	CC-FEA-01-2019-000795.R1
Article Type:	Feature Article

SCHOLARONE™
Manuscripts

Please do not adjust margins

ChemComm

FEATURE ARTICLE

Redox- and Light-Switchable N-Heterocyclic Carbenes: A "Soup-to-Nuts" Course on Contemporary Structure–Activity Relationships

Received 00th January 20xx,
Accepted 00th January 20xx

DOI: 10.1039/x0xx00000x

www.rsc.org/

Yeonkyeong Ryu, [a,b,†] Guillermo Ahumada, [a,b,†] and Christopher W. Bielawski [a,b,c,*]

Switchable catalysts respond to various types of stimuli in a manner that results in distinct structural or electronic changes. When each state exhibits a different activity, selectivity, or solubility, the corresponding catalyst may be used to control chemical reactions in a temporally- or spatially-resolved fashion. N-Heterocyclic carbenes are a versatile scaffold for building switchable catalysts and many examples that respond to changes in electrochemical potential or light have been introduced. Such types of switchable NHCs will be described in this Feature Article. The accompanying discussions include design considerations, characterization methodology, quantification of the underlying switching phenomena, and utility in catalytic applications. Challenges for the field as well as perspectives on potential opportunities for future development are also provided.

Introduction

Catalysis plays a critical role in the conversion of chemical feedstocks to valuable materials.[1,2] Many of the catalysts used in such transformations are designed to promote specific reactions or, in some cases, to synthesize specific substrates. As such, additional development and optimization efforts may be required after a catalyst is selected to maximize a desired result. Such efforts can range from solubility enhancements to refinement of steric and other structural parameters to the inclusion of additives or co-catalysts, among others.

Switchable catalysis offers a means to "switch" or toggle catalysts between multiple, distinct states, each of which may display a different type of activity, selectivity, solubility, or other performance characteristic.[3–7] Beyond expediting optimization schemes and potentially realizing "multi-tasking" systems that promote multiple, different transformations,[8] switchable catalysts offer a means to alter chemical reactions on demand. For example, polymerization reactions can be adjusted between "on" (active) and "off" (inactive) states using switchable catalysts,[9] which has enabled control with high temporal and, in some cases, spatial precision.[10] Likewise, polymerization catalysts with switchable monomer selectivities has facilitated access to new classes of structurally-advanced polymeric materials.[11,12] Control over transformations that produce mixtures of products may also be possible through the use of catalysts that exhibit switchable chemo- or stereoselectivities.[13,14]

Switchable catalysts typically feature functional groups that respond to external stimuli. When treated with an acid or base,[15–18] heated or cooled,[19] exposed to light,[20–23] oxidized or reduced,[24–31] or subjected to mechanical force,[32] the functional group experiences a change in structure or electronic property that ultimately modulates the activity and/or selectivity displayed by the attendant catalyst.[13] For reversible systems, removal of the stimulus or the introduction of a new stimulus should cause the catalyst to revert back to its initial form or to adopt a new one. Such features effectively facilitate access to multiple catalysts which maximizes potential versatility and control over chemical reactions, particularly when each catalyst uniquely performs.

N-Heterocycle carbenes (NHCs) are useful scaffolds for building switchable catalysts,[33–39] for multiple reasons: (1) NHCs are generally good nucleophiles and have been employed as organocatalysts[40–42] in a broad range of transformations; (2) akin to phosphines, NHCs serve as ligands for transition metals[43,44] and often enhance catalytic activity upon coordination;[34] (3) NHCs can be prepared using a multitude of established methodologies and appended[45] to essentially any functional group, including those that are stimuli-responsive;[46] and (4) NHCs are generally thermally stable, chemically robust, and can be outfitted with the appropriate N-substituents to facilitate isolation.[47,48]

This Feature Article provides an overview of switchable NHCs that have been introduced over the past several years. Emphasis will be placed on NHCs that respond to oxidizing/reducing environments (redox-switchable) or to light (photoswitchable) (e.g., see **1** – **4** in Figure 1) since the evolution and development of such systems have been well-

[a] Center for Multidimensional Carbon Materials (CMCM), Institute for Basic Science (IBS), Ulsan 44919 (Republic of Korea)
[b] Department of Chemistry, Ulsan National Institute of Science and Technology (UNIST), Ulsan 44919 (Republic of Korea)
[c] Department of Energy Engineering, Ulsan National Institute of Science and Technology (UNIST), Ulsan 44919 (Republic of Korea)
† These authors contributed equally to this work.
*Correspondence: bielawski@unist.ac.kr; Tel.: +82-52-217-2952

Please do not adjust margins

documented. Discussions will be generally presented in a chronological fashion and will include key design features, syntheses, characterization methodology, and deployment in various catalytic applications. The discourse will conclude with summary of the lessons learned over the course of these studies, suggestions for adaptation to other systems, challenges for the field, and a list of potential opportunities.

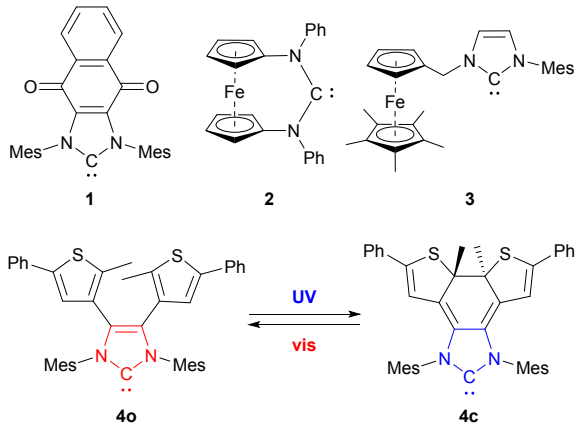

Figure 1. Examples of (top) redox- and (bottom) light-switchable NHCs.

Redox-Switchable NHCs

The first example of a redox-switchable catalyst based on an NHC scaffold was reported by Süßner and Plenio in 2005.[49] As shown in Figure 2, a derivative of the Hoveyda-Grubbs 2nd generation type catalyst (**5**) was designed to change its solubility in a manner that depended on the oxidation state of two pendant ferrocenyl groups connected to an imidazolylidene-base ligand. Cyclic voltammetry revealed that complex **5** exhibited oxidation processes at +0.410 V and +0.847 (vs. octamethylferrocene; $FcMe_8$), which were assigned to the Fe^{II}/Fe^{III} and Ru^{II}/Ru^{III} redox couples, respectively.

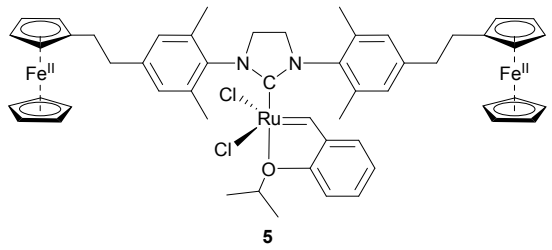

Figure 2. Example of a catalyst that undergoes a change in solubility upon oxidation of the redox-active NHC ligand.

The difference in electrochemical potential between the two processes indicated that the redox-active ligand may be selectively oxidized with an appropriate reagent. Indeed, the addition of acetylferrocenium triflate ($[AcFc]^+[OTf]^-$) at the conclusion of a ring-closing metathesis (RCM) reaction resulted in the oxidation of the redox-active groups, which effectively caused the catalyst to precipitate from solution. Filtration of the oxidized catalyst followed by treatment with an appropriate reductant (e.g., $FcMe_8$) restored the neutral form of catalyst, including its intrinsic solubility and activity. ^{1}H NMR experiments revealed that the integrity of the catalyst was intact after the oxidation/reduction sequence, even after multiple cycles, and quantitative yields of the expected RCM product were consistently achieved. Moreover, the rate of the reaction was fine-tuned by adding sub-stoichiometric amounts of the oxidation reagent with respect to the catalyst. Although attempts were made to effect catalyst deposition using bulk electrolysis, the electric current responses measured were reported to be too small to be practical.

The development of another class of redox-switchable NHCs began with an exploration of a quinone-annulated derivative (**1**).[50] The quinone / hydroquinone system is an established redox couple[51–53] and annulation to the backbone of an NHC was envisioned to facilitate communication between the redox-active center and the carbene nucleus (see Figure 3). In its neutral form, the NHC was predicted to be a relatively weak donor (or nucleophile) due to conjugation between the lone pair of electrons on the nitrogen atoms of the imidazolylidene and the carbonyl groups of the quinone moiety. Reduction was envisioned to disrupt communication between these two components which, in turn, should place more electron density on the carbene nucleus and render a better donor (or nucleophile). Intrinsic donor properties and/or nucleophilic characteristics may also be enhanced by the buildup of negative charge experienced by the carbene upon reduction.

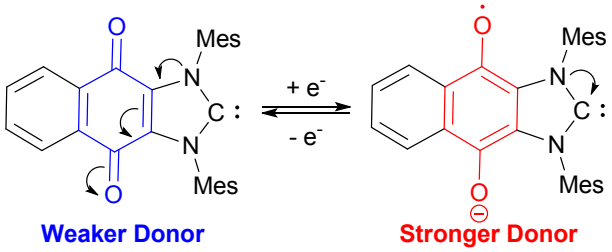

Figure 3. Hypothesized outcomes based on potential resonance contributors. The neutral form of the NHC was predicted to be a relatively weak donor whereas the reduced form was predicted to be relatively strong.

To test the hypothesis, Rh(I) complexes supported by the quinone-annulated NHC (**1**) and various diagnostic ligands (e.g., carbon monoxide) were synthesized and studied.[50] The NHC was prepared as a crystalline solid in two steps from commercially available materials, as shown in Figure 4, and then treated with $[RhCl(cod)]_2$ (cod = 1,5-cyclooctadiene). Carbonylation of the metallated product, (**1**)RhCl(cod) (**6**), afforded (**1**)$RhCl(CO)_2$ (**7**) (see Figure 5). FT-IR spectroscopy revealed that the cod complex exhibited a higher quinone carbonyl stretching frequency (υCO) than its carbonylated derivative (1680 cm^{-1} vs. 1670 cm^{-1}). The red-shifted value reflected the relative electron density on the metal center and

This journal is © The Royal Society of Chemistry 20xx

revealed that the quinone group was electronically communicating with the pendant ligands.

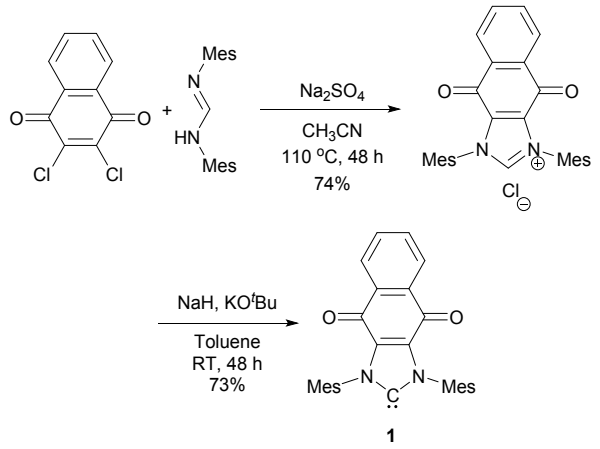

Figure 4. A synthetic route used to prepare the quinone-annulated NHC **1**.

Coupling between the metal center and the quinone group was further confirmed by measuring the reduction potentials of the aforementioned complexes. For example, the quinone group in **7** underwent reduction at -0.49 V (vs. Fc/Fc^+) whereas a larger value, -0.55 V, was recorded upon analysis of **6**. Even though the ancillary ligands were distal to the redox-active group, the reduction potentials agreed with the relative donating abilities of the ancillary ligands (cod vs. carbonyl).

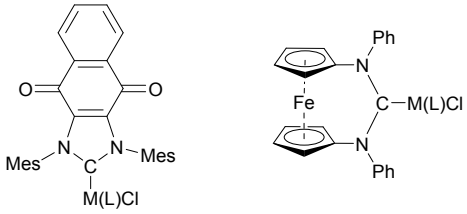

6: M = Rh; L = cod
7: M = Rh; L = 2(CO)
8: M = Ir; L = cod
9: M = Ir; L = 2(CO)
10: M = Rh; R = Ph; L = cod
11: M = Rh; R = Ph; L = 2(CO)
12: M = Rh; R = Neopentyl; L = cod
13: M = Rh; R = Neopentyl; L = 2(CO)

Figure 5. Structures of complexes of **1** and **2**, which feature redox-active quinone and ferrocene groups, respectively.

Since the υCOs displayed by Ir carbonyl complexes can be translated into Tolman Electronic Parameters (TEPs),[54] which are often used to measure the donor properties of supporting ligands,[55] including carbenes,[56,57] efforts were directed toward the synthesis and study of redox-active derivatives. The complexes were synthesized in a manner similar to that reported for the Rh complexes described above, where (**1**)IrCl(cod) (**8**) was prepared from the free NHC (**1**) and $[IrCl(cod)]_2$, and then carbonylated to form (**1**)$IrCl(CO)_2$ (**9**) (see Figure 5).[27] While **9** was found to exhibit υCO signals at 2072 cm^{-1} and 1988 cm^{-1}, the introduction of a reductant to the complex resulted in the formation of new signals at 2060 cm^{-1} and 1975 cm^{-1}.[27] Using averaged υCO values, TEPs of 2055.4 cm^{-1} and 2044.8 cm^{-1} were calculated for the neutral and reduced forms of the NHC, respectively. For comparison, TEP values of 2068.9 cm^{-1} and 2056.4 cm^{-1} have been reported for PPh_3 and PCy_3, which are often considered as relatively weak and strong donor ligands, respectively.[54] As another basis of comparison, the prototypical NHCs 1,3-dimesitylimidazolylidene (IMes) and dimesitylimidazolinylidene (SIMes) were reported to exhibit TEP values of 2023.1 cm^{-1} and 2024.6 cm^{-1}, respectively.[58] Collectively, these results indicated that the reduced form of the redox-active carbene (**1**) was a stronger donor than its neutral precursor.

Over the same period of time, a series of NHCs that featured integrated ferrocenyl units (**2**) were developed (see Figure 1),[59] in part to complement to the quinone-based analogue. Since the latter undergoes negative charge buildup upon reduction, carbenes that develop positive charge were envisioned to facilitate fundamental comparisons. The precursor of **2** was prepared through the formylative cyclization 1,1´-dianilinoferrocene[60] under acidic conditions.[59] Analogues that featured N-alkyl groups were prepared from N,N'-dialkylferrocene using similar methodology.

Similar to the approach used to study the quinone annulated NHC **1**, the ferrocene-containing NHC **2** was probed using (**2**)RhCl(cod) (**10**) and (**2**)$RhCl(CO)_2$ (**11**). Cyclic voltammetry revealed that the redox-active group in the carbonyl complex oxidized at a higher potential (+0.91 V) than the analogue containing cod (+0.54 V). The difference was attributed to the relative donating abilities of the ancillary ligands in conjunction with through-space interactions between the Fe center and the diaminocarbene moiety,[61] a conclusion that was supported by X-ray diffraction data collected for crystals of **10** and **11**. For example, the Fe–$C_{carbene}$ distance was measured to be longer in the carbonyl complex when compared to the analogue supported by cod (3.438(5) vs. 3.406(4) Å). An opposed trend was measured for the respective Rh–$C_{carbene}$ distances (2.044(4) vs. 2.081(3) Å), presumably due to compensation of the electronic differential.

To better ascertain how the ferrocenyl groups in **11** interacted with the ligated metal center, the carbonyl complexes were analyzed using FT-IR spectroscopy. Since the addition of various oxidants (e.g., iodine, iodosobenzoic acid, AgI, chloranil, or 2,3-dichloro-5,6-dicyano-1,4-benzoquinone; DDQ) to solutions of **11** resulted in decomposition, a method that used potentiostatic coulometry in conjunction with time-resolved IR spectroscopy was devised. As summarized in Figure 6, analysis showed that the stretching frequency of the CO ligand coordinated to the metal center was dependent on the oxidation state of the ferrocenyl group. For example, the υCO values increased from 2070 and 1992 cm^{-1} to 2088 and 2015 cm^{-1}, respectively, when a positive potential was applied (+0.9 V vs. SCE). The increments were attributed to the formation of stronger CO bonds due to the loss of electron density at the metal center as induced by the buildup of positive charge at the ferrocenyl group upon oxidation. These further established electronic coupling between the NHC and the metal center.

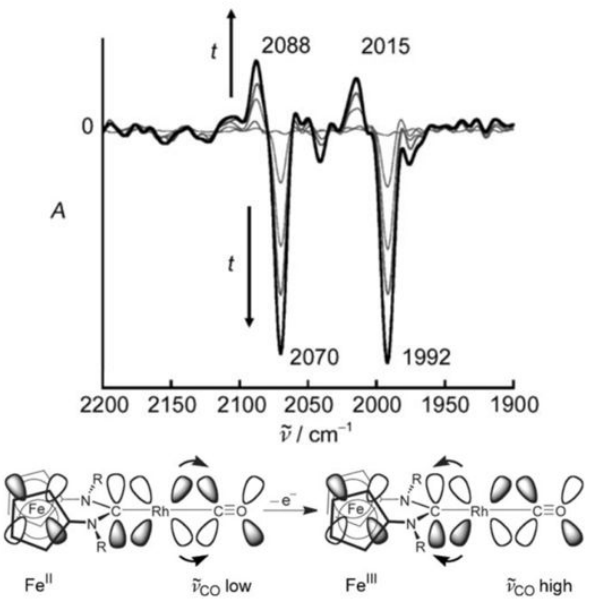

Figure 6. Top: Superimposed difference FT-IR spectra showing the disappearance of **11** (υCO = 2070, 1992 cm^{-1}) with concomitant formation of **11**$^{+}$ (υCO = 2088, 2015 cm^{-1}) upon oxidation (E = +0.9 V) over a duration of 200 s. Bottom: Graphical illustration explaining the effect of oxidizing **11** to **11**$^{+}$ on its carbonyl stretching frequency. The Rh moiety has been truncated for clarity; R = Ph. Adapted from ref. 59 with permission from John Wiley and Sons, copyright 2008.

Over the same period of time, a ferrocenophane-based NHC with relatively bulky N-substituents (neopentyl) was developed by Siemeling[62] and co-workers. The carbene was generated by deprotonating its formamidinium precursor, Fc[N(CH$_2$*t*Bu)-CH-N(CH$_2$*t*Bu)][BF$_4$], and then incorporated into Rh(I) complexes with the general formula of (NHC)RhCl(L) (L = (CO)$_2$ or cod) (see **12** and **13** in Figure 5). Similar conclusions regarding the relative electronics and donating properties of the redox-active NHC described above were deduced after analyzing **13**. For example, the $C_{carbene}$ atom in the complex exhibited a ^{13}C NMR signal at 184.0 ppm ($^{1}J_{Rh-C}$ 77.8 Hz; $CDCl_3$) and υCO signals assigned to the carbonyl groups were recorded at 2072 and 1993 cm^{-1}. These values indicated that the NHC was relatively electron rich and comparable to other strongly donating carbene-based ligands reported in the literature.[63] In addition, DFT calculations revealed that spin density was localized on the Fe and on the carbene nuclei upon oxidation of the NHC. The conclusion was in agreement with electron paramagnetic resonance (EPR) data where g values of 2.614 and 1.999 were ascertained and assigned to the presence of unpaired electrons at the Fe and carbene nuclei, respectively.[64] Collectively, these results indicated that the carbene center and the ferrocenyl groups were electronically coupled.

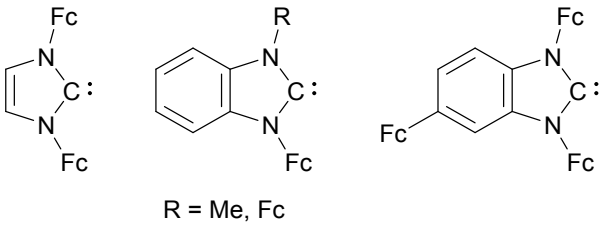

Figure 7. Structures of redox-active NHC ligands that were incorporated into metal complexes. Fc = ferrocenyl.

To explore how the carbene nuclei and ligated metal species were affected by the position and number of redox-active groups attached to the NHC scaffold, a systematic series containing different ferrocene units was synthesized (see Figure 7), and then incorporated into IrCl(cod), IrCl(CO)$_2$, or M(CO)$_5$ (M = Cr, Mo, W) complexes.[27] The complexes were characterized using a range of X-ray crystallography, spectroscopic, and electrochemical techniques. The changes in carbonyl stretching frequency that were recorded upon oxidation of the Ir carbonyl complexes were found to be similar (ΔυCO = +11 cm^{-1}), regardless of the location or the number of redox-active groups. The oxidation potentials measured for the Fe^{2+}/Fe^{3+} redox couples in the (NHC)IrCl(CO)$_2$ complexes were anodically shifted by 40 to 100 mV vs. decamethylferrocene (Fc*) when compared to their IrCl(cod) analogues. Similar to the differential IR data, the changes observed were comparable, regardless of the number or identity of the ferrocene units presented in the NHC. These results revealed how coulombic effects may contribute to the electronic interaction between the carbene nucleus and the redox-active groups.

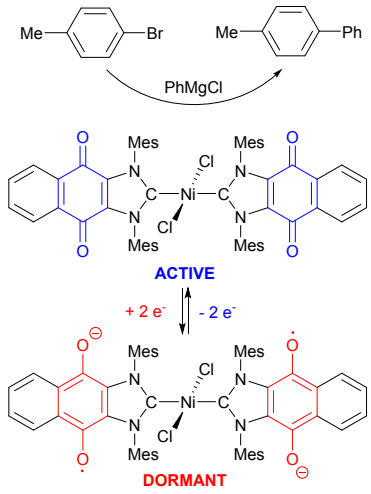

Figure 8. A switchable Ni complex supported by two quinone-annulated NHCs was used to control cross-coupling chemistry. The neutral form of the catalyst was found to be active yet transformed into a dormant state upon reduction.

After establishing and deciphering the communication between carbene nuclei and pendant redox-active groups,

This journal is © The Royal Society of Chemistry 20xx

efforts shifted toward exploring the redox-switchable NHCs in controlling synthetic transformations. Early emphasis was directed toward modulating Kumada cross-coupling reactions using a Ni(II) catalyst that was supported by the quinone-annulated NHC **1** (see Figure 8).[65] While the catalyst was found to be active in its neutral form, significantly lower activities were observed when the catalyst was treated with $CoCp_2$ (e.g., the observed rate constant, k_{obs}, changed from 4.7×10^{-5} s^{-1} to 2.7×10^{-6} s^{-1} upon reduction). Subsequent addition of an appropriate oxidant (e.g., $FcBF_4$) restored catalytic activity (k_{obs} = 1.2×10^{-5} s^{-1}). The difference in the measured rate constants was proposed to originate during transmetallation, which may become disfavored upon reduction of the NHC since the step entails bond formation between a negatively polarized carbon atom and an electron rich metal center. The catalyst was found to remain soluble upon reduction and thus activity changes due to precipitation were effectively ruled out.

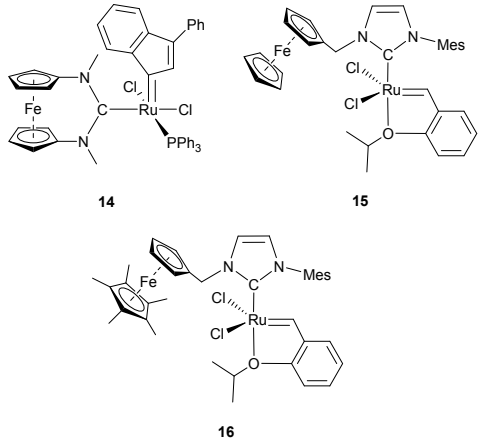

Figure 9. Structures of Ru-based olefin metathesis catalysts containing different redox-switchable NHCs.

Efforts were also directed toward controlling various olefin metathesis reactions using complexes that were outfitted with redox-switchable NHCs. A diaminocarbene[3]ferrocenophane ligand containing N-methyl substituents was incorporated into a Ru-based catalyst (**14**) (see Figure 9) and then used to modulate ring-opening metathesis polymerization (ROMP) reactions.[66] Cyclic voltammetry and differential pulse voltammetry revealed that the complex exhibited two quasi-reversible, overlapped processes at +0.79 and +0.98 V (vs. SCE), which were assigned to the Fe^{2+}/Fe^{3+} and Ru^{2+}/Ru^{3+} couples, respectively. While the neutral form of the catalyst was found to facilitate the ROMP of cod with a relatively high rate constant (k_{obs} = 0.045 s^{-1}), a lower value was measured (k_{obs} = 0.0012 s^{-1}) upon treatment with an oxidant (DDQ). Utilizing the activity differential, the rates of polymerization reactions were toggled between relatively "fast" and "slow" states by adding oxidants and reductants to the reaction mixture at various points in time. Switching performance was limited by the oxidized form of the catalyst (**14**$^+$), which appeared to be unstable. For example, adding reductant to a catalyst that spent 1 h in an oxidized state limited full recovery of the initial catalytic activity (k_{obs} = 0.0066 s^{-1}). Although improved restoration values were achieved by adding the reductant sooner (k_{obs} = 0.016 s^{-1}), the origin of the decomposition process was later attributed to inadvertent and irreversible oxidation of the Ru center (see below).

Further support for the formation of neutral and oxidized forms of the catalyst was obtained using UV-vis spectroscopy. Treatment of a CH_2Cl_2 solution of the catalyst with DDQ resulted in the appearance of signals at λ_{max} = 582, 542 and 344 nm, which were assigned to the $DDQ^{\cdot-}$ anion.[67] Although an additional absorption signal was observed at 620 nm, assignment of its origin as Fe or Ru (or both) was unambiguous due to the strong molar absorptivity of ferrocenium species.[68] A conclusion was reached upon EPR analysis of the oxidized complex. Paramagnetic species with g values of 4.29 and 2.01 were observed and assigned to the presence of Fe(III) and Ru(III) centers, respectively.[69] As noted above, formation of the latter may facilitate premature catalyst decomposition.

To explore how other redox-active NHCs that feature ferrocenyl groups performed in olefin metathesis chemistry, efforts were directed toward a Hoveyda-Grubbs 2nd generation catalyst (**15**) that was supported by 1-(ferrocenylmethyl)-3-mesitylimidazol-2-ylidene.[70] In its neutral form, the catalyst was measured to promote the RCM of diethyl diallylmalonate (DDM) at k_{obs} of 3.1×10^{-4} s^{-1}. However, upon oxidation (using acetylferrocenium tetrafluoroborate), the rate constant of the reaction was lowered by over an order of magnitude (1.2×10^{-5} s^{-1}, respectively). Attempts to reduce **15**$^+$ in situ were met with limited success, presumably because the Ru center underwent oxidation and resulted in premature decomposition. For example, only 13% of the initial catalytic activity was restored upon treating the oxidized catalyst with Fc*. Nevertheless, the RCM activity displayed by the catalyst was successfully switched between relatively "fast" and "slow" states, even after multiple cycles (see Figure 10).

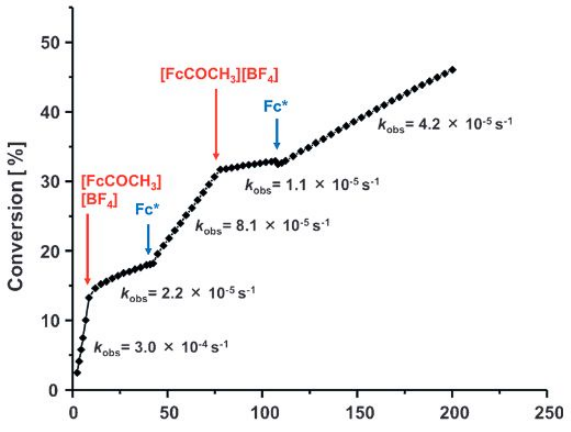

Figure 10. Plot of the percent conversion of DDM to product versus time as catalyzed by 1 mol % of **15**; conditions: $[DDM]_0$ = 0.1 M, CD_2Cl_2, 30 °C. The arrows indicate the time at which one equivalent of the stated reagent, with respect to **15**, was added. The corresponding rate constants over the given

periods of time are indicated. Adapted from ref. 70 with permission from John Wiley and Sons, copyright 2013.

It was predicted that increasing the electrochemical potential gap between the Fe^{2+}/Fe^{3+} and Ru^{2+}/Ru^{3+} redox couples would improve the switching performance. The hypothesis was tested with a relatively electron rich derivative, 1-(1,2,3,4,5-pentamethylferrocene)-3-mesitylimidazol-2-ylidene (**3**), which was incorporated into the Hoveyda-Grubbs 2nd generation catalyst (**16**). Cyclic voltammetry and dynamic pulse voltammetry indicated that the complex displayed redox couples at 0.36 V and 1.02 V (vs. SCE), which were assigned to the Fe and Ru centers, respectively (c.f., 0.62 V and 1.01 V for Ru^{2+}/Ru^{3+} for **15**). The wider electrochemical window enabled milder oxidants (and thus potentially more selective for ferrocene) to be employed and with improved outcomes. For example, the observed reaction rate constant was found to decrease from 4.5×10^{-5} s^{-1} to 0.86×10^{-5} s^{-1} upon the addition of acetylferrocenium tetrafluoroborate ($[FcCOCH_3][BF_4]$). Moreover, 94% of catalytic activity was successfully restored (k_{obs} = 4.25×10^{-5} s^{-1}) upon the subsequent addition of a suitable reductant (e.g., Fc*). These results indicated that selecting the appropriate oxidant and reductant may be of paramount importance, particularly for redox-active catalysts that exhibit multiple redox couples.

Amidst the development and deployment of Ru complexes supported by redox-active NHCs, Labande and co-workers[71] reported a Rh(I) complex that was ligated to a ferrocene-based heterodifunctional phosphine-NHC. Cyclic voltammetry revealed that the complex exhibited a reversible process at +0.35 V (vs. Fc/Fc^+) and an irreversible process at +0.95 V (vs. Fc/Fc^+). However, controlled potential electrolysis in CH_3CN at +0.49 V (vs. Fc/Fc^+) caused the metal center to intramolecularly C–H insert the ferrocenyl group and form a Rh(III) complex. The complex facilitated the arylation of 4-nitrobenzaldehyde via C–H activation of 2-phenylpyridine.[72]

To explore how redox-active NHCs that build negative charge influence olefin metathesis chemistry, a Ru-based 3rd generation Grubbs catalyst containing the quinone-annulated NHC (**17**) was synthesized and studied.[73] Cyclic voltammetry revealed that the complex exhibited a reversible reduction at -0.67 V (vs. SCE), which was assigned to the interconversion of the quinone and its semiquinone radical anion. Quantitative reduction was achieved using cobaltocene ($CoCp_2$) and the subsequent introduction of ferrocene hexafluorophosphate ($FcPF_6$) resulted in a 98% of recovery of the initial catalyst. The reversibility of the process was analyzed by FT-IR spectroscopy, where the salient carbonyl stretching frequency (υCO = 1752 cm^{-1}) disappeared upon reduction and re-appeared upon oxidation. Likewise, broad signals were observed by ^1H NMR spectroscopy upon treatment with $CoCp_2$, presumably due to paramagnetic effects. Regardless, spectral data matching those recorded for starting material (e.g., $\delta_{benzylidene}$ = 19.03 ppm; CD_2Cl_2) were observed upon subsequent treatment with DDQ. These results established an electronic connection between the NHC ligand and the Ru center and prompted an exploration of catalytic activity (see Figure 11).

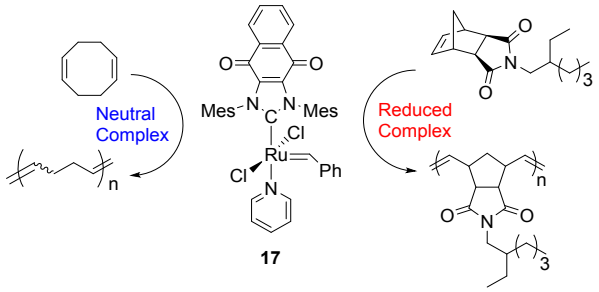

Figure 11. The neutral form of the Ru catalyst **17** was found to preferentially polymerize cod in its neutral form and a norbornene derivative in its reduced form.

While the neutral form of the complex was found to polymerize cod with a reaction rate constant ($k_{neutral}$) of 1.3×10^{-3} s^{-1}, significantly decreased activity ($k_{reduced}$ = 4.2×10^{-4} s^{-1}) was observed upon treatment of the catalyst with $CoCp_2$. However, an inverse effect was observed when a different monomer was utilized. The reduced form of the catalyst was found to be more active than its neutral precursor when a norbornene derivative was polymerized ($k_{reduced}$ = 6.2×10^{-4} s^{-1} vs. $k_{neutral}$ = 1.2×10^{-4} s^{-1}). The relative rate differences indicated that the selectivity of the catalyst was dependent on the oxidation state of the quinone-annulated NHC ligand. A series of a copolymerizations were performed wherein appropriate reductants and oxidants were added over time to finely tune the structure and compositions of the copolymers produced. The results showcased an advantageous feature of redox-switchable catalysts that exhibit state dependent monomer selectivities to control copolymerization reactions.[10,12,67]

To gain a deeper understanding of the intrinsic selectivities displayed by the aforementioned catalyst, a series of DFT analyses were performed. The rate-determining step for the ROMP of norbornene was calculated to be the [2+2] cycloaddition. The polymerization reaction may be promoted under such reducing conditions because the corresponding NHC ligand should more effectively stabilize the electron-deficient Ru(IV) intermediate than its neutral precursor. In contrast, the rate-determining step for the ROMP of cod was calculated to be cleavage of the ruthenacyclobutane. Since the reduced form of the NHC better stabilizes the Ru(IV) center than its neutral form, the retro-[2+2] cycloaddition is disfavored and thus a relatively slow reaction is observed under reducing conditions.[75]

A Ru-based Hoveyda-Grubbs second generation catalyst supported by the quinone-annulated NHC (**18**) was also synthesized and studied in a series of RCM reactions (see Figure 14).[25] The complex displayed a reversible process at -0.63 V (vs. SCE), which was attributed to the quinone/semiquinone redox couple. Similar to the experiments described above, adding $CoCp_2$ followed by $FcPF_6$ facilitated reduction and oxidation of the catalyst with high

This journal is © The Royal Society of Chemistry 20xx

Please do not adjust margins

fidelity (>95% conversions), even after multiple cycles, and a series of light scattering and ^{1}H NMR spectroscopy experiments indicated that the catalyst remained soluble upon reduction. The ability of the complex to undergo reversible reduction was confirmed by FT-IR spectroscopy as the intensity of carbonyl stretching frequency (υCO = 1674 cm^{-1}) disappeared upon the addition of reductant and then reformed upon subsequent treatment with an oxidant.

As summarized in Figure 12, the activity of the catalyst was also found to be dependent on the oxidation state of the quinone group. For example, a pseudo-first order rate constant for the RCM of DDM using the neutral form of the catalyst was measured to be $k_{neutral}$ = 2.0 × 10^{-4} s^{-1}. Reduction of the catalyst *in situ* resulted in a markedly decreased catalytic activity; $k_{reduced}$ = 3.0 × 10^{-5} s^{-1}. Moreover, the catalyst was toggled between states of high and low activity over the course of a single reaction by adding the appropriate oxidant or reductant at various points in time. Similar trends were observed with other substrates, including diethyl (2-methylallyl)(allyl)malonate, 1,7-octadiene and 1,7-heptadiene. DFT analyses revealed that the activity changes stem from the differential donating properties of the NHC. The reduced form of the ligand stabilizes the ruthenacyclobutane intermediates and thus suppresses the rate-determining retro-[2+2] cycloaddition step.

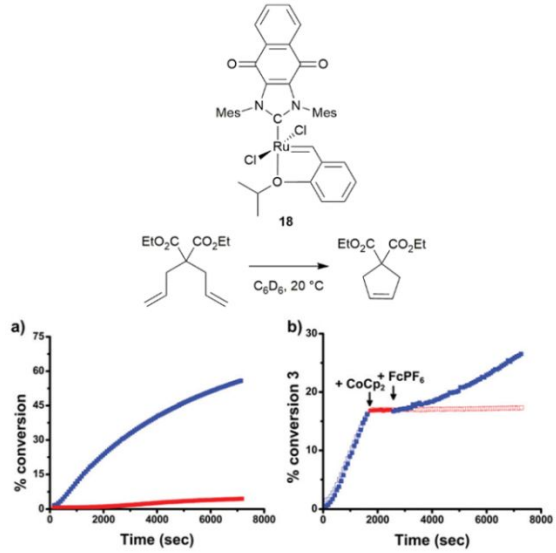

Figure 12. (a) Plots of percent conversion of DDM to product vs. time as initiated with **18** (blue) or in situ generated **18$_{red}$** (red). (b) After initiating the reaction with **18**, $CoCp_2$ or $FcPF_6$ were added at the indicated times. Conditions: $[DDM]_0$ = 0.02 M, $[DDM]_0/[\mathbf{18}$ or $\mathbf{18}_{red}]_0$ = 100, 5 : 1 v/v C_6D_6/CD_2Cl_2, 20 °C. Adapted from ref. 25 with permission from the Royal Society of Chemistry, copyright 2017.

Chen and co-workers[76] recently showed that metal complexes supported by the quinone-based redox-active ligand described above and its derivatives may be also used to control olefin addition polymerizations. The Pd complexes **19** described in Figure 13 were found to undergo reversible reductions at approximately -0.6 V (vs. Ag/AgCl), consistent with the analogous metal complexes supported by **1**. Likewise, the polymerization activities displayed by the catalysts were found to be dependent on the oxidation state of the ligand. The neutral form of the catalyst was activated with sodium [tetrakis(3,5-bis fluoromethyl)phenyl)borate] (to facilitate halide abstraction), and used to polymerize norbornene, 5-norbornene-2-yl acetate and 1-chloro-1-octyne. While lower catalytic activities were measured upon reduction of the NHC ligand with $CoCp_2$, initial activity was restored upon treatment of the reduced catalyst with a suitable oxidant (e.g., ferrocene tetrakis(3,5-bis(trifluoromethyl)phenyl)borate). Although the underlying mechanism is still being investigated,[77] it is hypothesized that increasing electron density at the catalytically-active metal center disfavors monomer coordination or key propagation steps.

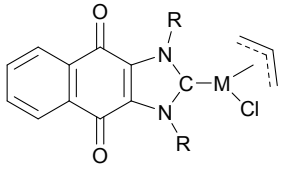

19

R = 2,6-Me_2-C_6H_3
R = 2,6-^{i}Pr$_2$-C_6H_3

Figure 13. Structures of quinone annulated NHC-Pd complexes that were used to control olefin addition polymerizations.

Mirkin and co-workers[78] recently reported a redox-switchable tweezer that featured a Pt(II) complex supported by a NHC connected via a thioether ferrocenyl unit. As shown in Figure 14, oxidation of the redox-active group in **20** using bulk electrolysis (0.38 V vs. Fc/Fc$^+$) or through the addition of a suitable reagent (e.g., $AgBF_4$) to the reaction mixture changed the coordination sphere of the metal center in a manner that enabled ligation to the thioether; subsequent reduction reversed the reaction. Such features effectively blend redox chemistry with allosteric regulation,[79] and thus are expected to be useful for selectively activating and deactivating specific catalytic processes on demand.

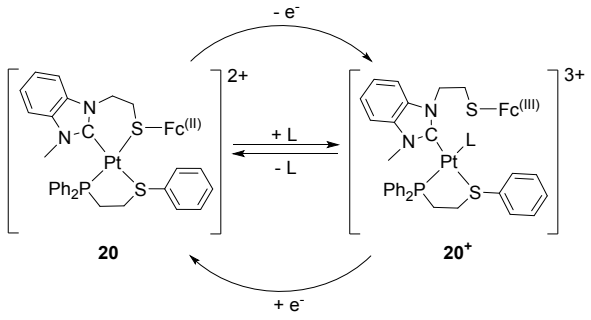

Figure 14. Oxidation of **20** was shown to change the coordination sphere of the complex. L = thioanisole.

Photoswitchable NHCs

The first example of a photoswitchable NHC was based on a diarylethene (DAE). DAEs are not only widely used photochromic compounds, due to their synthetic accessibility and good resistance to fatigue, but are also known to undergo electrocyclization and ring-opening upon exposure to UV and visible light, respectively.[80] In 2009, Yam and co-workers reported the synthesis of a series of imidazolium salts that contained DAEs as part of their backbones and ligated the deprotonated derivatives (i.e., the respective NHCs) to Au(I), Ag(I), or Pd(II) centers (see Figure 15).[81] Analysis of the complexes using UV-vis absorption spectroscopy revealed that they exhibited strong signals at approximately 230 nm, which were attributed to the π → π* transitions of the N-heterocycle and the n → π* transitions of the thiophene groups. The observation of new absorption signals at 320-350 nm and 520-570 nm upon exposure of the complexes to UV light were consistent with data reported for other DAEs.[80,82–86]

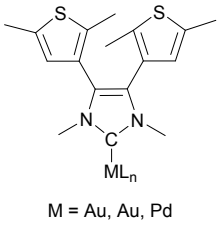

Figure 15. DAE-annulated NHC supported metal complexes.

It was reasoned that annulating a diarylethene to the backbone of an NHC scaffold would provide a means to change or "switch" the intrinsic reactivity and/or electron donating ability of the carbene nucleus through photochemistry (see Figure 16). Inspection of the canonical structure of the ring-opened form of the NHC indicated that the imidazolylidene unit was cross-conjugated with the thiophenyl units. As a result, electron donation from the nitrogen atoms to the carbene nucleus should be favored and thus increase the donating and nucleophilic properties of the corresponding NHC. Ring-closure was expected to engage coupling between the lone pairs of electrons on the nitrogen atoms and the electronegative sulfur atoms. Electron density from the carbene nucleus should decrease accordingly and afford an NHC that is relatively electrophilic and/or weakly donating.

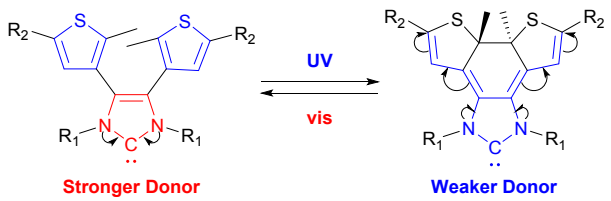

Figure 16. Hypothesized outcomes based on potential resonance contributors. The ring-opened form of the NHC was predicted to be a relatively strong donor whereas the ring-closed form was predicted to be relatively weak.

The hypothesis was initially tested using a series of NHC-chalcogen adducts (see Figure 17).[87] Distinct color changes were observed upon irradiating solutions of the ureas with UV light (λ = 280 nm) as the colorless reaction mixtures turned to orange or red, consistent with the formation of an electrocyclized, conjugated product (e.g., **21c** or **22c**). In parallel, the extent of the reaction was quantified using UV-vis spectroscopy (see Figure 18). Isomerization of the oxygen adduct **21c** resulted in the disappearance of an absorption signal at 214 nm concomitant with the appearance of new signal at 476 nm. Moreover, an isosbestic point (255 nm) was identified upon monitoring the reaction over time which reflected the high fidelity of the photocyclization process. Within 10 min of UV irradiation, the chalcogen adducts reached their photostationary states and approximately 75% of the starting materials were converted to their ring-closed forms. Subsequent exposure to visible light (λ > 500 nm) resulted in a loss in color and restored the UV-vis spectrum recorded for the starting material (90% conversion). The ring-closing and ring-opening processes were found to be reversible and proceeded with minimal decomposition (<10%).

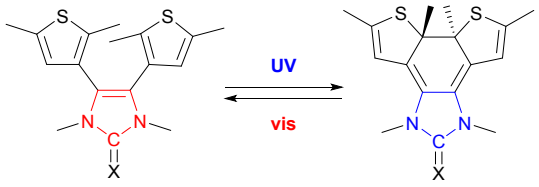

Figure 17. Structures of photoswitchable NHC-chalcogen and metal adducts.

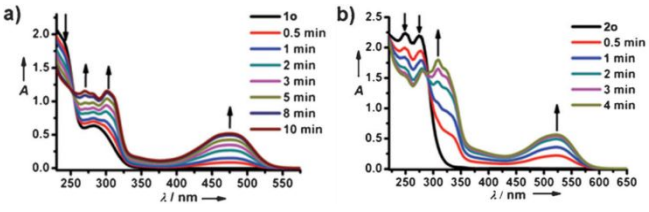

Figure 18. (a) UV/Vis spectral changes of **21o** in acetonitrile ([**21o**]$_0$ = 10^{-4} M) upon UV irradiation (λ = 280 nm). The spectra were recorded after irradiation for the indicated period of time. (b) UV/Vis spectral changes of **22o** in acetonitrile ([**22o**]$_0$ = 10^{-4} M) upon UV irradiation (λ = 280 nm). The spectra were recorded for the indicated period of time. Adapted from ref. 87 with permission from John Wiley and Sons, copyright 2011.

A variety of other techniques were employed to confirm the reversible photocyclization process and to validate the aforementioned hypothesis. As shown in Figure 19, the carbonyl stretching frequency recorded for the oxygen adduct **21** hypsochromically shifted by 28 cm^{-1} (from 1688 cm^{-1} to

This journal is © The Royal Society of Chemistry 20xx

1716 cm^{-1}) upon photocyclization. The thiocarbonyl stretching frequency of the sulfur adduct **22** was less pronounced (< 2 cm^{-1}) due to the increased reduced mass of the two-body system. These results indicated that the ring-opened form of the NHC was relatively donating and effectively weakened the C=X bond. In contrast, the ring-closed form siphoned electron density away from the carbene nucleus which caused the C=X bond to become stronger.

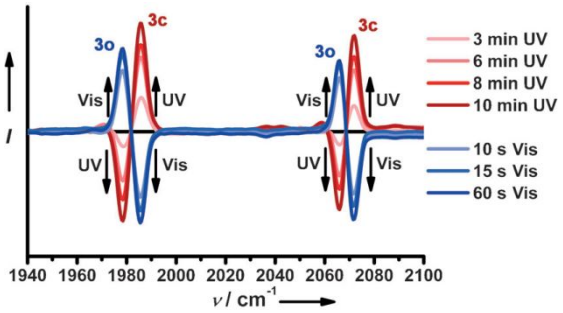

Figure 19. Data in red: Normalized infrared difference spectra that were recorded as **23o** (2066 and 1978 cm^{-1}) was converted to **23c** (2072 and 1986 cm^{-1}) in cyclohexane ([**23o**]$_0$ = 10^{-2} M). Data in blue: Normalized infrared difference spectra that were recorded as **23c** (2072 and 1986 cm^{-1}) was converted to **23o** (2066 and 1978 cm^{-1}). The arrows indicate the evolution of the spectral changes over time. Reproduced from ref. 87 with permission from John Wiley and Sons, copyright 2011.

The ring-closed form of **21c** was sufficiently stable such that it could be isolated (62% yield) and independently characterized. The ^{13}C NMR spectrum recorded for the product revealed a diagnostic signal at 67.8 ppm ($CDCl_3$) that was assigned to the methine carbons bonded to the sulfur atoms and provided additional support for the cyclization reaction. The NHC adduct was found to remain in its ring-closed form for more than 24 h when kept in the solid-state or in solution (chloroform, toluene or hexanes), and for weeks when chilled (-20 °C). The isolated adduct was subsequently ring-opened upon irradiation with visible light (λ > 500 nm) for 3 min or upon the exposure to ambient light for 3 h.

The structures of the ring-opened and ring-closed forms of the oxygen adducts were further elucidated using data obtained from an X-ray diffraction analysis (see Figure 20). The interplanar distortion angle between the thiophene and imidazole rings was measured at 57.3(3)° for **21o** and 16.40(12)° for **21c**, indicating that a relatively planar structure formed in the latter upon ring-closure. Likewise, the vicinal methyl groups were found to adopt a *trans*-configuration, consistent with the outcome expected for an electrocyclization reaction.

A series of Ir complexes containing the photoswitchable NHC (**23**) were evaluated after the chalcogen adducts described above. As expected for an electrocyclization reaction, irradiating a solution of **23o** in cyclohexane with UV light (λ = 297 nm) resulted in the disappearance of an absorption signal centered at 227 nm and the formation of a new signal at 545 nm over the same period of time. The cyclization was further supported in part by the observation of a new ^{1}H NMR signal at 5.38 ppm (C_6D_6), which was assigned to the annulated dihydrothiophene. While FT-IR analysis of **23** revealed that the complex exhibited carbonyl stretching frequencies at 2066 and 1978 cm^{-1}, the values shifted to 2072 and 1986 cm^{-1}, respectively, upon photocyclization. The corresponding TEPs for the ring-opened and ring-closed forms of the NHC were calculated to be 2049 cm^{-1} and 2055 cm^{-1}, respectively.[54]

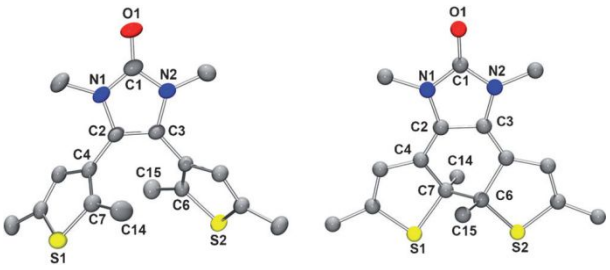

Figure 20. POV-ray representations of the solid-state structures of **23o** (left) and its cyclized derivative **23c** (right) showing ellipsoids at 50% probability. Hydrogen atoms have been omitted for clarity. Reproduced from ref. 87 with permission from John Wiley and Sons, copyright 2011.

After these initial reports, the aforementioned photoswitchable NHC scaffold underwent several iterations and design optimizations to improve performance (see Figure 21). First, the methyl groups located in the 2-positions of the thiophene rings were substituted with phenyl groups to extend conjugation such that relatively low energy light could be utilized to effect cyclization (280 nm vs. 313 nm) and to minimize potential side or decomposition reactions.[88] Second, bulky mesityl groups were attached to the nitrogen atoms of the imidazolylidene to prevent dimerization of the free carbene and to facilitate isolation.[89,90]

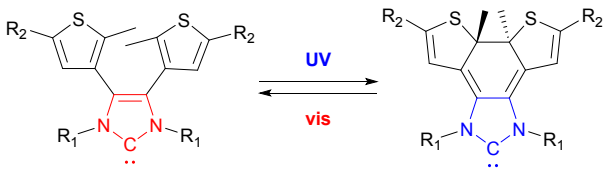

24o, **25o**, **4o** **24c**, **25c**, **4c**

Generation 1: **24** (R_1: CH_3; R_2: CH_3)
Generation 2: **25** (R_1: CH_3; R_2: Ph)
Generation 3: **4** (R_1: Mes; R_2: Ph)

Figure 21. Evolution of the structures of photoswitchable NHCs.

The precursor to the first generation photoswitchable NHC can be synthesized by condensing 2,5-dimethylthiophene with oxalyl chloride followed by the formylative cyclization and methylation. Figure 22 summarizes pathways that have been used to synthesize 2nd and 3rd generation photoswitchable

NHCs.[88,90] Syntheses generally begin with 2-methyl-5-phenylthiophene, which can be acylated with acetic anhydride in the presence of tin (IV) chloride to afford 3-acetyl-2-methyl-5-phenylthiophene (**a**). Treating **a** with selenium dioxide affords the geminal diol **b**, which can be coupled with 2-methyl-5-phenylthiophene. Oxidation of the acyloin product (**c**) with copper (II) acetate or 2-iodoxybenzoic acid (IBX) yields the corresponding 1,2-diones (**d**). If the targeted N-substituents are 1° alkyl groups, then amination followed by formylative cyclized affords the corresponding imidazole (**e**), which can then be substituted upon treatment with the appropriate alkyl halide (**f**). Note: Anion exchange is typically performed because iodide precursors were discovered to undergo premature decomposition under UV light. If the targeted N-substituents are aryl groups, then the corresponding 1,2-diimine (**g**) should be prepared prior to formylative cyclization (**h**). Treatment of the imidazolium salts with a strong base, such as potassium *tert*-butoxide (KO^{t}Bu) or sodium hexamethyldisilazide (NaHMDS), affords the corresponding free NHCs.

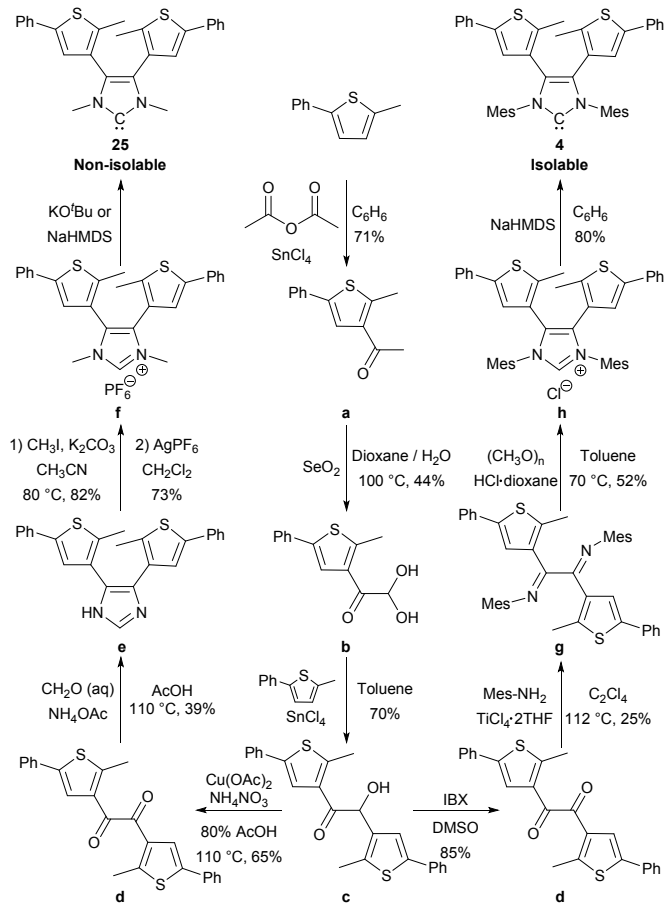

Figure 22. Synthetic routes used to prepare non-isolable and isolable photoswitchable NHCs.

The first design improvement facilitated control over transesterifications and amidations.[88] NHCs have been used to catalyze such condensation chemistry and are typically generated in situ from their protonated precursors.[42,91–93] Building upon these established reactions, the photocyclization of **25** (generated in situ) and its precursors was monitored using UV-vis and ^{1}H NMR spectroscopy. The UV-vis spectra recorded for **25o** exhibited intense absorptions between 275 and 325 nm, which were assigned to the n → π* transitions of the NHC and the π → π* transitions of the thiophene groups. Upon exposure to UV light (λ = 313 nm), the signal centered at 292 nm decreased and a new signal centered at 670 nm grew in intensity. The process was accompanied with a color change as a benzene solution of **25o** turned from a pale yellow to a bright blue. Likewise, ^{1}H NMR signals assigned to the thiophene units shifted upfield (from 7.3 ppm to 6.9 ppm; CD_3CN) as did the proton at the 2-position of the imidazolium (from 8.6 ppm to 8.1 ppm) until an 81% conversion to **25c** was reached. Subsequent exposure of **25c** to ambient light for 4 h recovered **25o** (>95% conversion). Since the active catalysts in the aforementioned condensation reactions are free NHCs, UV-vis experiments were also conducted under basic conditions and results similar to those obtained for the imidazolium precursors described above were obtained.

The transesterification of allyl alcohol with vinyl acetate and the amidation of ethyl acetate with 2-aminoethanol were separately explored using the photoswitchable carbene as a catalyst. The NHC was generated in situ by treating its protonated precursor with an appropriate base (KO^{t}Bu or NaHMDS). The rate constants for the reactions performed under visible light were measured to be similar (c.f., k_{vis} = 5 ± 1 × 10^{-4} $mol^{-1}{\cdot}s^{-1}$ for the transesterification vs. 5 ± 4 × 10^{-4} $mol^{-1}{\cdot}s^{-1}$ for the amidation). However, significantly slower kinetics were observed (k_{UV} = 4 ± 1 × 10^{-5} $mol^{-1}{\cdot}s^{-1}$ vs. 5 ± 4 × 10^{-6} $mol^{-1}{\cdot}s^{-1}$, respectively) when the reactions were conducted under UV light (λ = 313 nm). Inspection of the data revealed that the activity displayed by ring-opened form of the NHC was approximately one order of magnitude higher than that of its ring-closed isomer (k_{vis}/k_{UV} = 10) when used as a transesterification catalyst and two orders of magnitude higher when used to promote amidations (k_{vis}/k_{UV} = 100).

To better understand how light influenced the aforementioned changes in activity, a series of ^{13}C NMR experiments in conjunction with isotopically labeled NHCs (to enhance diagnostic signals) were performed. A summary of the conclusions derived from those experiments is shown in Figure 23. While the ring-opened form of the NHC functioned as expected of a nucleophilic carbene catalyst, the ring-closed isomer was sufficiently electrophilic such that it reacted alkoxides that were generated during the condensation reactions. The resulting adducts were found to be stable and effectively removed the catalyst from the catalytic cycle. Subsequent irradiation of the reaction mixture with visible light caused the adducts to undergo ring-opening which effectively expelled the alkoxides and regenerated nucleophilic NHCs that could re-engage the catalytic cycle.

This journal is © The Royal Society of Chemistry 20xx

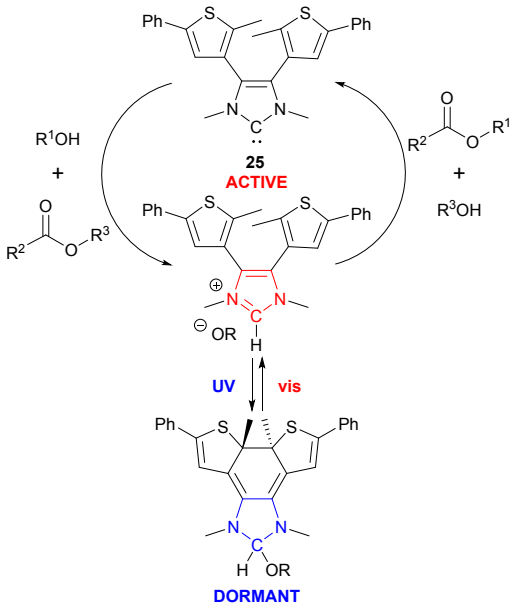

Figure 23. A proposed condensation mechanism as catalyzed by a photoswitchable NHC.

While the DAE was being developed, Monkowius and co-workers introduced (2013) a photoswitchable NHC scaffold that employed a photochromic azobenzene (see Figure 24).[94] UV irradiation (λ = 323 nm and 351 nm) of Au(I) complex **26** facilitated the familiar E → Z isomerization,[20,95] as determined by UV-vis spectroscopy. For example, absorption data recorded for the E isomer showed a strong absorption at 320 nm, which was assigned to a π → π* transition, and a weak absorption at > 400 nm, which was assigned to a n → π* transition. Upon irradiation with UV light, the absorption of relatively high energy transitions (220 – 330 nm) decreased while lower-energy bands (430 nm) increased. The reverse reaction, which typically proceeds via thermally induced processes, was found to be relatively slow. Half-lives ($\tau_{1/2}$) were reported to be 6400 min at room temperature and 90 min at 90 °C. These results established a new type of photoswitchable NHC that may provide control over molecular structure and electronics in ways that differ from those displayed by the DAEs.

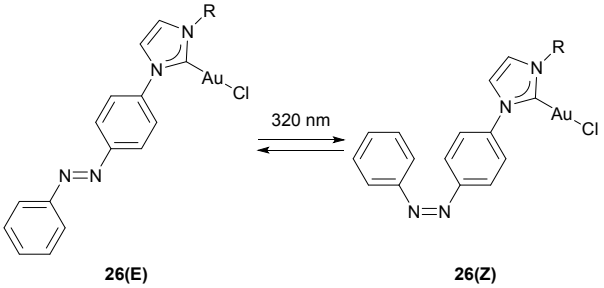

Figure 24. Photoinduced E-to-Z isomerization of an azobenzene-containing NHC-metal complex.

Since NHCs have also been established as useful catalysts for ring-opening polymerization (ROP) reactions,[91,96] it was hypothesized that the photoswitchable NHC described above may be used to control such chemistry. Similar to the transesterifications described above, **25** (generated in situ) catalyzed the polymerization of δ-valerolactone when benzyl alcohol was used as an initiator and the reaction was performed under visible light. However, irradiating the reaction mixture with UV light (λ = 313 nm) to generate the ring-closed form of the catalyst (**25c**) resulted in a markedly decreased activity (k_{vis}/k_{UV} = 59). Moreover, the rate of the polymerization reaction was successfully toggled between relatively "slow" and "fast" states through alternate exposure to UV and visible light, respectively (see Figure 25). The mechanism of ROP with the photoswitchable NHC was elucidated and found to be similar to the transesterification chemistry described above.

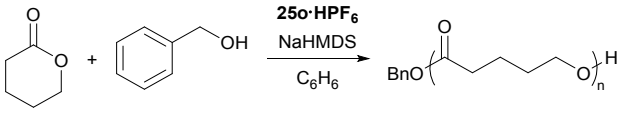

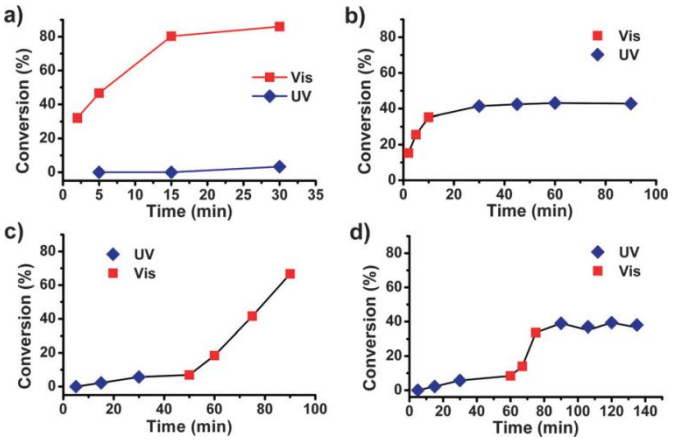

Figure 25. Plots of reaction conversion versus time for the ROP of δ-valerolactone as catalyzed by **25** (prepared in situ from **25·HPF$_6$** and NaHMDS) in C_6H_6. Conditions: $[\delta\text{-valerolactone}]_0$ = 0.5 M; $[BnOH]_0/[\mathbf{25o}]_0$ = 4; $[\delta\text{-valerolactone}]_0/[\mathbf{25o}]$ = 250, unless otherwise noted. The reactions were performed under UV (λ = 313 nm; blue diamonds) or visible light light (red squares). Reproduced from ref. 96 with permission from the Royal Society of Chemistry, copyright 2013.

The photoswitchable NHC was also used to catalyze the ROP of ε-caprolactone. Under ambient light, **25o** converted more than 95% of the monomer to polymer within a few minutes. In contrast, performing the same reaction under UV light showed less than 5% conversion. Due to the rapid polymerization kinetics, the ROP of ε-caprolactones was found to be practically challenging to modulate in a temporal manner. To demonstrate how the catalyst may be used to control such polymerizations, a photogated experiment was

devised. Once a polymerization reaction reached completion and afforded a polymeric material (number average degree of polymerization, M_n = 12,500 Da), the reaction mixture was exposed to UV light and then charged with additional monomer. The freshly added monomer did not undergo consumption and a significant change in polymer molecular weight was not observed, even after 3 h. However, subsequent exposure of the mixture to visible light restored catalytic activity and produced a larger polymer (M_n = 19,000 Da). While photocyclization effectively "gated" (i.e., placed into a dormant state) growing polymer chains, re-activation occurred upon ring-opening. These results demonstrated a new method for controlling fast polymerization reactions which may find utility in certain applications (e.g., injection molding) and, in a broader context, constituted an early example of a photoswitchable NHC-based polymerization catalyst.

Photoswitchable NHCs have also been used to control metal-catalyzed reactions.[97] A Rh-based hydroboration catalyst (**27**) was synthesized by adding Ag_2O and $[RhCl(cod)]_2$ to the corresponding NHC precursor. Before exploring the utility of the catalyst, UV-vis spectroscopy experiments were performed to evaluate the underlying photoswitchable characteristics. The UV-vis spectrum recorded for **27o** showed intense signals that were centered at 285 nm and assigned to the n → π* transitions of the NHC and the π → π* transitions of the phenylthiophene groups. Upon UV irradiation (λ = 313 nm), the signal at 285 nm disappeared as new signals at 391 nm and 630 nm formed. From the spectroscopic data, it was determined that 64% of **27o** converted to **27c** under UV light and that 98% of the initial complex was recovered after exposure to visible light. The identification of an isosbestic point (311 nm) provided further support for the reversibility of the photochemical reaction.

Having established that complex **27** undergoes reversible isomerization, it was explored as a hydroboration catalyst. 1-Octene, styrene and *tert*-butylacetylene were selected as substrates and pinacolborane was used as the hydroboration reagent. The hydroboration of 1-octene, as promoted by **27o** under visible light, was monitored over time and a rate constant of k_{vis} = 1.9 ± 0.5 × 10^{-3} $mol^{-1}{\cdot}s^{-1}$ was measured. For comparison, a significantly lower rate constant, k_{UV} = 7.8 ± 2.1 × 10^{-4} $mol^{-1}{\cdot}s^{-1}$ (k_{vis}/k_{UV} = 2.4), was determined when the same reaction was performed using **27c**, which was generated in situ with UV light. The hydroboration of styrene was also found to proceed with a higher rate constant under visible light, although the difference in activities was larger (k_{vis}/k_{UV} = 9.2). As a result, the rate of the reaction was successfully switched between "slow" and "fast" states over time through alternate exposure to UV and visible light, respectively. Similar results were obtained with 4-chlorostyrene (k_{vis}/k_{UV} = 6.5), 4-methoxystyrene (k_{vis}/k_{UV} = 7.7), and *tert*-butylacetylene (k_{vis}/k_{UV} = 3.7). As shown in Figure 26, if the rate determining step of the reaction is reductive elimination, then complexes supported by the ring-opening form should feature less electron density at the metal center and thus result in a lower rate of reaction.

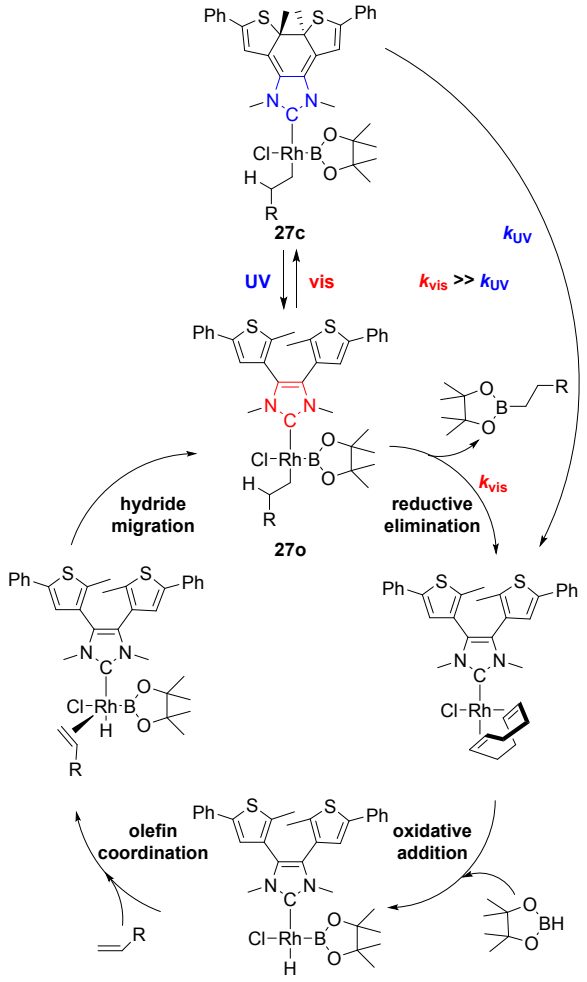

Figure 26. A proposed hydroboration mechanism as catalyzed using a photoswitchable NHC. Adapted from ref. 97 with permission from the American Chemical Society, copyright 2013.

An isolable form of the photoswitchable NHC (**4**) was reported in 2015 which, from a practical perspective, facilitated characterization and utility.[90] As shown in Figure 27, UV-vis spectroscopic data recorded for the NHC as well as its ring-closed form were similar to the analogues described above that required in situ generation. The ring-opened formed of the NHC (**4o**) exhibited a diagnostic absorption signal at 293 nm, which decreased in intensity upon exposure to UV light (λ = 313 nm). The process was accompanied by the formation of a new signal at 328 nm and reached a photostationary state after 60 seconds of irradiation of UV light (54% conversion). Isosbestic points were identified which indicated that the photocyclization process proceeded without significant side reactions or decomposition. Likewise, distinct color changes (pale yellow to deep purple) were visually observed upon exposing solutions of the free carbene to UV light. Subsequent irradiation with visible light (λ > 500 nm) showed a decrease in the low energy absorptions as well as

This journal is © The Royal Society of Chemistry 20xx

decoloration, as expected for the corresponding ring-opening reaction.

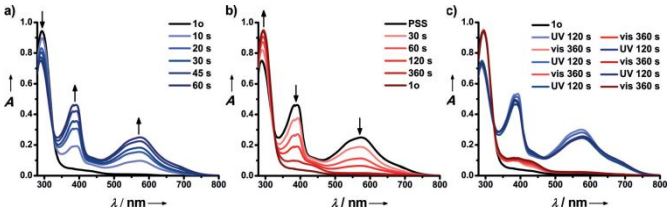

Figure 27. (a) UV/Vis spectral changes of **4o** in C_6H_6 upon UV irradiation (λ = 313 nm). (b) UV/Vis spectrum of the photostationary state (PSS) reached after UV irradiation of **4o** for 60 s, and spectral changes of the PSS over time upon visible-light irradiation (λ>500 nm). The arrows point to the evolution of spectral changes ($[\mathbf{4o}]_0$=3.5 × 10^{-5} M). (c) UV/Vis spectral changes of **4o** in C_6H_6 ($[\mathbf{4o}]_0$=3.5 × 10^{-5} M) upon successive UV (λ = 313 nm) and visible-light (λ>500 nm) irradiation. The spectra were recorded after 120 s and 360 s, respectively (indicated). Reproduced from ref. 90 with permission from John Wiley and Sons, copyright 2015.

The ^{13}C NMR signals of carbene nuclei in NHCs are strongly dependent on the electronic characteristics of their scaffolds.[48,89] As such, it was reasoned that the ability to isolate NHC **4** should facilitate the determination of the chemical shifts of the carbene nuclei and enable a direct comparison between the ring-opened and ring-closed forms of the free carbene. Unfortunately, preliminary experiments indicated that the ^{13}C NMR signals displayed by the carbene nuclei in **4** were too weak to be clearly identified. To enhance signal intensity, an isotopically enriched derivative was prepared by using $(^{13}CH_2O)_n$ in the formylative cyclization step described in Figure 22. As shown in Figure 28, the carbene nucleus of the ^{13}C-enriched derivative of **4o** exhibited a signal at 219.5 ppm (C_6D_6) whereas its ring-closed form, which was prepared in situ by exposing the reaction mixture to UV light, the displayed a signal 243.5 ppm. Subsequent exposure to visible light effectively reversed the reaction. The difference in chemical shifts provided reflected the relative electronic properties of the two isomers of **4**.

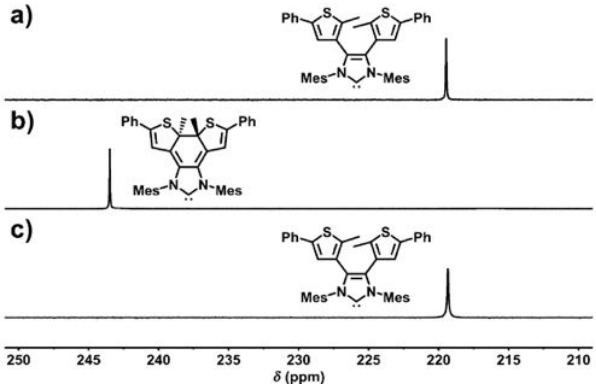

Figure 28. ^{13}C NMR spectra recorded in C_6D_6 for a sample of ^{13}C-labeled **4o** (a) before and (b) after exposure to UV light for 60 min (λ = 313 nm, [^{13}C-labeled **4o**]$_0$ = 1.0 × 10^{-3} M), followed by (c) irradiation with visible light for 3 h (λ>500 nm). Reproduced from ref. 90 with permission from John Wiley and Sons, copyright 2015.

Since a photoswitchable NHC that exhibited relatively electron rich characteristics in the ring-opened form and relatively electron deficient characteristics in the ring-closed form was prepared, it was proposed that the nucleophilicity of the carbene should follow suit. To test this hypothesis, ammonia was chosen as a test substrate because it is known that N–H insertion occurs when electron deficient carbenes are used.[98–101] No reaction was observed upon mixing **4o** and NH_3 in C_6D_6. However, irradiating the reaction mixture with UV light resulted in the rapid formation of an NHC-NH_3 adduct (see Figure 29), which was determined in part by the observation of a diagnostic ^{1}H NMR signal at 5.68 ppm (t, **H**-C-NH_2) and 1.28 ppm (d, H-C-N**H$_2$**). Subsequent exposure of the solution to visible light caused the adduct to dissociate and returned the NHC as well as ammonia (-0.17 ppm). Moreover, the reaction turned from pale yellow to dark purple as the carbene underwent N–H insertion with ammonia and the initial color was restored upon dissociation of the adduct. The hypothesis was further supported through a series of molecular orbital calculations, which showed that the carbene nucleus of **4o** was a component of the HOMO and that **4c** exhibited a pronounced LUMO at the carbene nucleus.

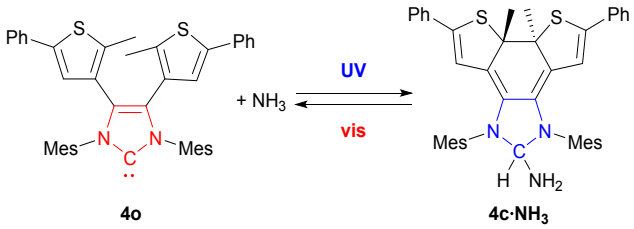

Figure 29. An example of using a photoswitchable NHC to reversibly activate ammonia.

The isolable carbene also facilitated access to new photoswitchable metal complexes. A ruthenium-based metathesis catalyst supported by the photoswitchable NHC (**28**)[102] was synthesized by adding the free NHC to the 1st generation Hoveyda-Grubbs catalyst (HG1). The UV-vis spectra of the complex exhibited an intense absorption signal centered at 298 nm, which was attributed to the n → π* transitions of the NHC and the π → π* transitions of the phenylthiophene groups. Upon UV irradiation (λ = 313 nm), the band centered at 298 nm disappeared while new bands at 453 nm and 639 nm formed. The color of the catalyst was also found to change from a deep blue-green to pale green over the same period of time. Based on the UV-vis data, it was determined that the photocyclization reaction reached 68% conversion in 7 min, and the retro-photocyclization restored 91% of the initial complex within 9 min. As shown in Figure 30, the salient benzylidene ^{1}H NMR signal shifted upfield from 16.97 ppm to 16.66 ppm in C_6D_6 upon photocyclization, and a relatively high (80%) conversion was reached, presumably due to the

increased concentration of the experiment. Regardless, subsequent irradiation with visible light (λ > 500 nm) for 1 h fully restored the initial ^{1}H NMR spectrum of the complex.

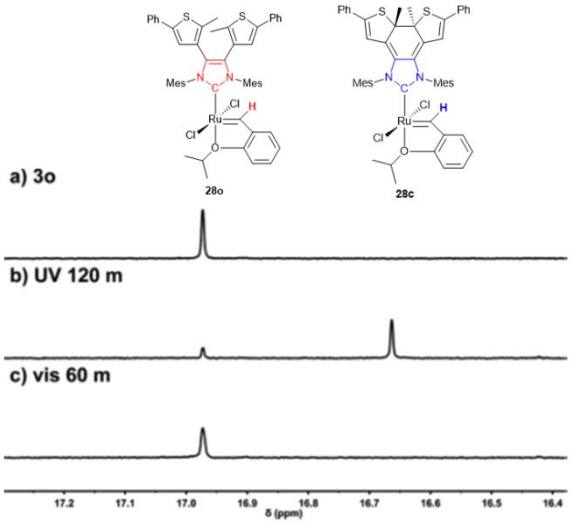

Figure 30. ^{1}H NMR spectra recorded in C_6D_6 of (a) **28o**, (b) after exposure to UV light (λ = 313 nm) for 120 min, and (c) subsequently exposure to visible light (λ > 500 nm) for 60 min ([**28o**]$_0$ = 1.0 × 10^{-3} M). Adapted from ref. 102 with permission from the American Chemical Society, copyright 2017.

After characterizing the photoswitchable Ru complex, its ability to control ring-closing metathesis and ring-opening metathesis polymerization reactions was explored. Under UV light, the catalyst converted DDM to its expected product at a higher rate constant (k_{UV} = 3.0 ± 0.1 × 10^{-4} s^{-1}) than the value calculated from analogous experiments performed under visible light (k_{vis} = 2.1 ± 0.2 × 10^{-4} s^{-1}) (k_{UV}/k_{vis} = 1.4). An opposite trend was observed when the catalyst was used to promote ROMP reactions. While the conversions of cod or norbornene derivatives to their respective polymers were measured to proceed at rate constants of 1.7 ± 0.1 × 10^{-3} s^{-1} and 2.5 ± 0.2 × 10^{-3} s^{-1}, respectively, under visible light, lower rate constants were measured when the polymerization reactions were conducted under UV light (1.12 ± 0.03 × 10^{-3} s^{-1} and 1.4 ± 0.1 × 10^{-3} s^{-1}, respectively) (k_{UV}/k_{vis} = 0.66 to 0.56).

Three sets of DFT calculations were conducted to gain a deeper understanding of the activity differences. (1) The RCM reaction featured a ruthenacyclobutane intermediate as the resting state and a retro-[2+2] cycloaddition as the rate-determining step. Since the Ru(IV) in the former may stabilized by the relatively strong donating properties of the ring-opened form of the NHC, the energy barrier of the reaction involving **28o** was found to be relatively high. (2) While the retro-[2+2] cycloaddition was also calculated to be the rate-determining step for the ROMP of cod, **28o** was found to lower the barrier of the retro-[2+2] cycloaddition when compared to that of **28c** due to steric interactions between the metal center and the growing polymer chains. (3) In contrast, the [2+2] cycloaddition was calculated to be the rate-determining step for the ROMP of norbornene. As such, the ruthenacyclobutane intermediates may stabilized by strongly donating ligands (c.f., **28o** vs. **28c**) in a manner that facilitates the reaction.

Summary

Redox-switchable NHCs outfitted with groups designed to undergo reduction or oxidation have been developed. The NHCs were evaluated in part through their metal carbonyl complexes wherein υCO values and other key spectroscopic data were found to vary with the oxidation state of the redox-active groups. Refinement of the constituent electronic interactions was obtained through electrochemical and analytical measurements. The data provided a qualitative and quantitative assessment of how the NHCs experience a change in their intrinsic properties upon undergoing reduction or oxidation. Such fundamental information guided the utility of redox-switchable NHCs in a broad range of catalytic reactions. In some cases, catalysts that were supported by redox-switchable NHCs underwent an enhancement in activity upon reduction (e.g., cross-coupling and RCM reactions) whereas, in other cases, activity was found to increase upon oxidation (e.g., ROMP). Control over substrate selectivity was achieved through oxidation state changes as well. In many of these examples, the redox-active NHCs were switched between different states, often repeatedly, which enabled modulation over the attendant chemical reactions.

Photoswitchable NHCs have been largely based on DAE scaffolds, although new systems (e.g., azobenzene) are beginning to emerge. By examining complexes with various chalcogens and metal complexes, it was determined that the ring-opened forms of such NHCs are relatively strong donors whereas the ring-closed forms are relatively weak. The changes in the donicity and accompanying nucleophilicity were used to control various catalytic reactions. In some cases (e.g., ring-opening polymerizations, transesterifications/amidations, and hydroborations), an enhancement in activity was observed when catalysts that featured the ring-opened form of the NHC were used. In other cases (e.g., NH_3 activation and RCM reactions), catalysts that were supported by the ring-closed form proved to be more active. Reversible photochemistry that proceeded with high fidelity was observed in many of the photoswitchable NHCs and associated complexes which, like the redox-switchable systems described above, enhanced control over chemical transformations.

Collectively, the results described in this Feature Article provide a continuous link from design to evaluation to application, which should facilitate the development of future iterations and adaptations. The stimuli used in conjunction with the switchable NHCs described above are also warrant consideration.[103] For example, many catalysts, particularly those that are based on metal complexes, display activities that are strongly dependent on their electronic properties. As such, the redox-switchable NHCs may be broadly applied.[3] Another attractive feature of redox-based approaches is that the switching processes may be executed electrochemically[2] or using the plethora chemical oxidants and reductants currently available.[53] Light is also an appealing stimulus for use in

This journal is © The Royal Society of Chemistry 20xx

switchable catalysis because it can be harnessed from multiple sources, filtered, and conveniently introduced with high spatial and temporal resolution.

Challenges and Opportunities

The redox- and light-switchable NHCs have undergone several iterations of advancement, which have improved performance and enhanced practicality. While early versions needed to be generated in situ and/or required high energy light to facilitate electrocyclization, recent variants have proven to be isolable and may be used under relatively benign conditions. Even though the study and application of switchable NHCs has expanded, a number of challenges remain. For example, the majority of the switchable NHCs that have been reported thus far are monodentate, which may preclude access to complexes that require multidentate ligands.[104] Although reduced and oxidized forms of the NHCs have been generated and characterized in situ, their isolation remains difficult, potentially due to side reactions that may occur upon concentration. Since judicious selection of the reagents used with the redox-switchable NHCs can be imperative to avoid inadvertent side reactions, the use of bulk electrochemical techniques may offer a solution, although appropriate solvents and electrolytes need to be explored and diffusion limitations may preclude fast switching rates.

Despite the challenges, opportunity abounds. An ability to impart electronic changes at the carbene nuclei that are greater than those reported may significantly enhance the effects observed and result in catalysts with unsurpassed activities or selectivities. Switchable NHCs that are capable of adopting more than two states may also offer new levels of control. One may envision fusing the redox- and light-switchable systems or merging them with functional groups that respond to other types of stimuli.[44,46] Access to the photoswitchable NHCs are generally multi-step endeavors and thus further synthetic improvements may expedite the preparation of such types of NHCs or their derivatives. Finally, NHCs are known to coordinate to nearly all metals[34,47,48] and can be used independently as organocatalysts.[40,105–109] Thus, while a number of catalytic reactions have been explored, the potential of using redox- and light-switchable NHCs to control other chemical transformations remains extraordinarily high.

Conflicts of interest

There are no conflicts to declare.

Acknowledgements

The Institute for Basic Science (IBS-R019), the Office of Naval Research (N00014-14-1-0650), and the BK21Plus Program as funded by the Ministry of Education and the National Research Foundation of Korea are acknowledged for support. We are grateful to Ms. Younghye Park for creating the graphical abstract.

Biographies

Yeonkyeong Ryu received a B.S. degree in energy engineering from UNIST in 2016. During her undergraduate studies, she joined the research group of Prof. Bielawski and began exploring applications in the area of redox-switchable catalysis. She received a M.S. degree in chemistry (2019) and is currently working toward a PhD degree.

Guillermo Ahumada received a B.S. degree in chemistry (2012) from the Pontificia Universidad Católica de Valparaiso (PUCV), Chile, and a Ph.D. degree (2017) in cotutelle between the PUCV (Chile) and the Université de Rennes 1 (France) under the supervision of Prof. Carolina Manzur and Prof. Jean-René Hamon, focusing on the electrosynthesis of metal containing polymers. Upon finishing his Ph.D., he began a postdoctoral appointment in the laboratories of Prof. Bielawski.

Christopher W. Bielawski received a B.S. degree in chemistry from the University of Illinois, Urbana-Champaign and a Ph.D. degree from the California Institute of Technology. After a postdoctoral appointment (also at Caltech), he assumed an independent position at the University of Texas at Austin, where he directed numerous projects rooted in organic, organometallic, and polymer chemistry. After about a decade in Texas, he launched a new research initiative in South Korea on the synthesis and study of macromolecular materials.

This journal is © The Royal Society of Chemistry 20xx

Notes and references

1 T. Welton, *Chem. Rev.*, 1999, **99**, 2071–2084.

2 K. Matyjaszewski and J. Xia, *Chem. Rev.*, 2001, **101**, 2921–2990.

3 U. Lüning, *Angew. Chem. Int. Ed.*, 2012, **51**, 8163–8165.

4 A. J. McConnell, C. S. Wood, P. P. Neelakandan and J. R. Nitschke, *Chem. Rev.*, 2015, **115**, 7729–7793.

5 G. Zhan, W. Du and Y.-C. Chen, *Chem. Soc. Rev.*, 2017, **46**, 1675–1692.

6 Y. Yağci and I. Reetz, *Prog. Polym. Sci.*, 1998, **23**, 1485–1538.

7 F. A. Leibfarth, K. M. Mattson, B. P. Fors, H. A. Collins and C. J. Hawker, *Angew. Chem. Int. Ed.*, 2013, **52**, 199–210.

8 I. M. Lorkovic, R. R. Duff and M. S. Wrighton, *J. Am. Chem. Soc.*, 1995, **117**, 3617–3618.

9 C. K. A. Gregson, V. C. Gibson, N. J. Long, E. L. Marshall, P. J. Oxford and A. J. P. White, *J. Am. Chem. Soc.*, 2006, **128**, 7410–7411.

10 A. J. Teator, D. N. Lastovickova and C. W. Bielawski, *Chem. Rev.*, 2016, **116**, 1969–1992.

11 A. B. Biernesser, B. Li and J. A. Byers, *J. Am. Chem. Soc.*, 2013, **135**, 16553–16560.

12 X. Wang, A. Thevenon, J. L. Brosmer, I. Yu, S. I. Khan, P. Mehrkhodavandi and P. L. Diaconescu, *J. Am. Chem. Soc.*, 2014, **136**, 11264–11267.

13 G. Romanazzi, L. Degennaro, P. Mastrorilli and R. Luisi, *ACS Catal.*, 2017, **7**, 4100–4114.

14 S. M. Shepard and P. L. Diaconescu, *Organometallics*, 2016, **35**, 2446–2453.

15 H. J. Yoon, J. Kuwabara, J.-H. Kim and C. A. Mirkin, *Science*, 2010, **330**, 66–69.

16 J.-F. Lefebvre, M. Lo, D. Leclercq and S. Richeter, *Chem. Commun.*, 2011, **47**, 2976–2978.

17 J.-F. Lefebvre, J.-F. Longevial, K. Molvinger, S. Clément and S. Richeter, *C. R. Chim.*, 2016, **19**, 94–102.

18 J. Beswick, V. Blanco, G. De Bo, D. A. Leigh, U. Lewandowska, B. Lewandowski and K. Mishiro, *Chem. Sci.*, 2015, **6**, 140–143.

19 O. Coulembier, A. P. Dove, R. C. Pratt, A. C. Sentman, D. A. Culkin, L. Mespouille, P. Dubois, R. M. Waymouth and J. L. Hedrick, *Angew. Chem. Int. Ed.*, 2005, **117**, 5044–5048.

20 R. S. Stoll and S. Hecht, *Angew. Chem. Int. Ed.*, 2010, **49**, 5054–5075.

21 B. M. Neilson and C. W. Bielawski, *ACS Catal.*, 2013, **3**, 1874–1885.

22 T. Wu and N. R. Branda, *Chem. Commun.*, 2016, **52**, 8636–8644.

23 D. Bléger and S. Hecht, *Angew. Chemie Int. Ed.*, 2015, **54**, 11338–11349.

24 M. Qi, Q. Dong, D. Wang and J. A. Byers, *J. Am. Chem. Soc.*, 2018, **140**, 5686–5690.

25 D. N. Lastovickova, A. J. Teator, H. Shao, P. Liu and C. W. Bielawski, *Inorg. Chem. Front.*, 2017, **4**, 1525–1532.

26 E. M. Broderick, N. Guo, C. S. Vogel, C. Xu, J. Sutter, J. T. Miller, K. Meyer, P. Mehrkhodavandi and P. L. Diaconescu, *J. Am. Chem. Soc.*, 2011, **133**, 9278–9281.

27 E. L. Rosen, C. D. Varnado, A. G. Tennyson, D. M. Khramov, J. W. Kamplain, D. H. Sung, P. T. Cresswell, V. M. Lynch and C. W. Bielawski, *Organometallics*, 2009, **28**, 6695–6706.

28 E. L. Rosen, C. D. Varnado, K. Arumugam and C. W. Bielawski, *J. Organomet. Chem.*, 2013, **745**–**746**, 201–205.

29 S. Dadashi-Silab, F. Lorandi, M. Fantin and K. Matyjaszewski, *Chem. Commun.*, 2019, **55**, 612–615.

30 W. C. Anderson, J. L. Rhinehart, A. G. Tennyson and B. K. Long, *J. Am. Chem. Soc.*, 2016, **138**, 774–777.

31 O. R. Luca and R. H. Crabtree, *Chem. Soc. Rev.*, 2013, **42**, 1440–1459.

32 A. Piermattei, S. Karthikeyan and R. P. Sijbesma, *Nat. Chem.*, 2009, **1**, 133–137.

33 S. P. Nolan and Wiley InterScience (Online service), *N-Heterocyclic carbenes in synthesis*, Wiley-VCH, Weinheim, Germany, 2006.

34 S. Díez-González, N. Marion and S. P. Nolan, *Chem. Rev.*, 2009, **109**, 3612–3676.

35 A. S. K. Hashmi, C. Lothschütz, K. Graf, T. Häffner, A. Schuster and F. Rominger, *Adv. Synth. Catal.*, 2011, **353**, 1407–1412.

36 S. Ibáñez, M. Poyatos and E. Peris, *ChemCatChem*, 2016, **8**, 3790–3795.

37 S. Ibáñez, M. Poyatos, L. N. Dawe, D. Gusev and E. Peris, *Organometallics*, 2016, **35**, 2747–2758.

38 M. Ruamps, S. Bastin, L. Rechignat, A. Sournia-Saquet, D. A. Valyaev, J.-M. Mouesca, N. Lugan, V. Maurel and V. César, *Chem. Commun.*, 2018, **54**, 7653–7656.

39 F. E. Hahn and M. C. Jahnke, *Angew. Chem. Int. Ed.*, 2008, **47**, 3122–3172.

40 N. Marion, S. Díez-González and S. P. Nolan, *Angew. Chem. Int. Ed.*, 2007, **46**, 2988–3000.

41 M. Fèvre, J. Pinaud, Y. Gnanou, J. Vignolle and D. Taton, *Chem. Soc. Rev.*, 2013, **42**, 2142–2172.

42 D. M. Flanigan, F. Romanov-Michailidis, N. A. White and T. Rovis, *Chem. Rev.*, 2015, **115**, 9307–9387.

43 W. A. Herrmann and C. Köcher, *Angew. Chem. Int. Ed.*, 1997, **36**, 2162–2187.

44 S. Kuwata and F. E. Hahn, *Chem. Rev.*, 2018, **118**, 9642–9677.

45 L. Benhamou, E. Chardon, G. Lavigne, S. Bellemin-Laponnaz and V. César, *Chem. Rev.*, 2011, **111**, 2705–2733.

46 E. Peris, *Chem. Rev.*, 2018, **118**, 9988–10031.

47 D. Bourissou, O. Guerret, F. P. Gabbaï and G. Bertrand, *Chem. Rev.*, 2000, **100**, 39–92.

48 T. Dröge and F. Glorius, *Angew. Chem. Int. Ed.*, 2010, **49**, 6940–6952.

49 M. Süßner and H. Plenio, *Angew. Chem. Int. Ed.*, 2005, **44**, 6885–6888.

50 M. D. Sanderson, J. W. Kamplain and C. W. Bielawski, *J. Am. Chem. Soc.*, 2006, **128**, 16514–16515.

51 M. Bauscher and W. Maentele, *J. Phys. Chem.*, 1992, **96**, 11101–11108.

52 J. Q. Chambers, in *The Quinonoid Compounds: Vol. 1 (1988)*, John Wiley & Sons, Inc., Chichester, UK, pp. 719–757.

53 N. G. Conelly and W. E. Geiger, *Chem. Rev.*, 1996, **96**, 877–

This journal is © The Royal Society of Chemistry 20xx

910.
54 C. A. Tolman, *Chem. Rev.*, 1977, **77**, 313–348.
55 D. Cremer and E. Kraka, *Dalton Trans.*, 2017, **46**, 8323–8338.
56 R. H. Crabtree, in *The Organometallic Chemistry of the Transition Metals*, John Wiley & Sons, Inc., Hoboken, NJ, USA, 2005, pp. 87–124.
57 H. V. Huynh, *Chem. Rev.*, 2018, **118**, 9457–9492.
58 B. J. A. van Weerdenburg, S. Glöggler, N. Eshuis, A. H. J. Engwerda, J. M. M. Smits, R. de Gelder, S. Appelt, S. S. Wymenga, M. Tessari, M. C. Feiters, B. Blümich and F. P. J. T. Rutjes, *Chem. Commun.*, 2013, **49**, 7388–7390.
59 D. M. Khramov, E. L. Rosen, V. M. Lynch and C. W. Bielawski, *Angew. Chem. Int. Ed.*, 2008, **47**, 2267–2270.
60 U. Siemeling, T.-C. Auch, O. Kuhnert, M. Malaun, H. Kopacka and B. Bildstein, *Z. Anorg. Allg. Chem.*, 2003, **629**, 1334–1336.
61 J. Silver, *Dalton Trans.*, 1990, **0**, 3513–3516.
62 U. Siemeling, C. Färber, M. Leibold, C. Bruhn, P. Mücke, R. F. Winter, B. Sarkar, M. von Hopffgarten and G. Frenking, *Eur. J. Inorg. Chem.*, 2009, **2009**, 4607–4612.
63 S. Wolf and H. Plenio, *J. Organomet. Chem.*, 2009, **694**, 1487–1492.
64 J. A. Kramer and D. N. Hendrickson, *Inorg. Chem.*, 1980, **19**, 3330–3337.
65 A. G. Tennyson, V. M. Lynch and C. W. Bielawski, *J. Am. Chem. Soc.*, 2010, **132**, 9420–9429.
66 C. D. Varnado, Jr., E. L. Rosen, M. S. Collins, V. M. Lynch and C. W. Bielawski, *Dalton Trans.*, 2013, **42**, 13251–13264.
67 H. M. A. Salman, M. R. Mahmoud, M. H. M. Abou-El-Wafa, U. M. Rabie and R. H. Crabtree, *Inorg. Chem. Commun.*, 2004, **7**, 1209–1212.
68 R. Prins, *J. Chem. Soc. D.*, 1970, **0**, 280b–281.
69 T. Sixt, J. Fiedler and W. Kaim, *Inorg. Chem. Commun.*, 2000, **3**, 80–82.
70 K. Arumugam, C. D. Varnado, S. Sproules, V. M. Lynch and C. W. Bielawski, *Chem. Eur. J.*, 2013, **19**, 10866–10875.
71 A. Labande, N. Debono, A. Sournia-Saquet, J.-C. Daran and R. Poli, *Dalton Trans.*, 2013, **42**, 6531–6537.
72 L. Yang, C. A. Correia and C.-J. Li, *Adv. Synth. Catal.*, 2011, **353**, 1269–1273.
73 D. N. Lastovickova, H. Shao, G. Lu, P. Liu and C. W. Bielawski, *Chem. Eur. J.*, 2017, **23**, 5994–6000.
74 C. Chen, *ACS Catal.*, 2018, **8**, 5506–5514.
75 H. Martinez, P. Miró, P. Charbonneau, M. A. Hillmyer and C. J. Cramer, *ACS Catal.*, 2012, **2**, 2547–2556.
76 W. Zou, W. Pang and C. Chen, *Inorg. Chem. Front.*, 2017, **4**, 795–800.
77 M. Chen, B. Yang and C. Chen, *Angew. Chem. Int. Ed.*, 2015, **54**, 15520–15524.
78 H. F. Cheng, A. I. d'Aquino, J. Barroso-Flores and C. A. Mirkin, *J. Am. Chem. Soc.*, 2018, **140**, 14590–14594.
79 L. Kovbasyuk and R. Krämer, *Chem. Rev.*, 2004, **104**, 3161–3188.
80 M. Irie, *Chem. Rev.*, 2000, **100**, 1685–1716.
81 V. W. Yam, J. K. Lee, C. Ko and N. Zhu, *J. Am. Chem. Soc.*, 2009, **131**, 912–913.
82 V. W. W. Yam, C. C. Ko and N. Zhu, *J. Am. Chem. Soc.*, 2004, **126**, 12734–12735.
83 C. C. Ko, W. M. Kwok, V. W. W. Yam and D. L. Phillips, *Chem. Eur. J.*, 2006, **12**, 5840–5848.
84 T. W. Ngan, C. C. Ko, N. Zhu and V. W. W. Yam, *Inorg. Chem.*, 2007, **46**, 1144–1152.
85 P. H. M. Lee, C. C. Ko, N. Zhu and V. W. W. Yam, *J. Am. Chem. Soc.*, 2007, **129**, 6058–6059.
86 C.-C. Ko, W. H. Lam and V. Wing-Wah Yam, *Chem. Commun.*, 2008, **0**, 5203–5205.
87 B. M. Neilson, V. M. Lynch and C. W. Bielawski, *Angew. Chem. Int. Ed.*, 2011, **50**, 10322–10326.
88 B. M. Neilson and C. W. Bielawski, *J. Am. Chem. Soc.*, 2012, **134**, 12693–12699.
89 A. C. Hillier, W. J. Sommer, B. S. Yong, J. L. Petersen, L. Cavallo and S. P. Nolan, *Organometallics*, 2003, **22**, 4322–4326.
90 A. J. Teator, Y. Tian, M. Chen, J. K. Lee and C. W. Bielawski, *Angew. Chem. Int. Ed.*, 2015, **54**, 11559–11563.
91 N. E. Kamber, W. Jeong, R. M. Waymouth, R. C. Pratt, B. G. G. Lohmeijer and J. L. Hedrick, *Chem. Rev.*, 2007, **107**, 5813–5840.
92 G. A. Grasa, R. M. Kissling and S. P. Nolan, *Org. Lett.*, 2002, **4**, 3583–3586.
93 G. W. Nyce, J. A. Lamboy, E. F. Connor, R. M. Waymouth and J. L. Hedrick, *Org. Lett.*, 2002, **4**, 3587–3590.
94 M. Kaiser, S. P. Leitner, C. Hirtenlehner, M. List, A. Gerisch and U. Monkowius, *Dalton Trans.*, 2013, **42**, 14749–14756.
95 M. Vlatković, B. S. L. Collins and B. L. Feringa, *Chem. Eur. J.*, 2016, **22**, 17080–17111.
96 B. M. Neilson and C. W. Bielawski, *Chem. Commun.*, 2013, **49**, 5453–5455.
97 B. M. Neilson and C. W. Bielawski, *Organometallics*, 2013, **32**, 3121–3128.
98 G. D. Frey, V. Lavallo, B. Donnadieu, W. W. Schoeller and G. Bertrand, *Science*, 2007, **316**, 439–441.
99 J. P. Moerdyk, G. A. Blake, D. T. Chase and C. W. Bielawski, *J. Am. Chem. Soc.*, 2013, **135**, 18798–18801.
100 T. W. Hudnall and C. W. Bielawski, *J. Am. Chem. Soc.*, 2009, **131**, 16039–16041.
101 U. Siemeling, C. Färber, C. Bruhn, M. Leibold, D. Selent, W. Baumann, M. Von Hopffgarten, C. Goedecke and G. Frenking, *Chem. Sci.*, 2010, **1**, 697–704.
102 A. J. Teator, H. Shao, G. Lu, P. Liu and C. W. Bielawski, *Organometallics*, 2017, **36**, 490–497.
103 V. Blanco, D. A. Leigh and V. Marcos, *Chem. Soc. Rev.*, 2015, **44**, 5341–5370.
104 J.-C. Hierso, R. Smaliy, R. Amardeil and P. Meunier, *Chem. Soc. Rev.*, 2007, **36**, 1754–1769.
105 K. Zeitler, *Angew. Chem. Int. Ed.*, 2005, **44**, 7506–7510.
106 D. Enders, O. Niemeier and A. Henseler, *Chem. Rev.*, 2007, **107**, 5606–5655.
107 V. Nair, S. Vellalath and B. P. Babu, *Chem. Soc. Rev.*, 2008, **37**, 2691–2698.
108 V. Nair, R. S. Menon, A. T. Biju, C. R. Sinu, R. R. Paul, A. Jose and V. Sreekumar, *Chem. Soc. Rev.*, 2011, **40**, 5336–5346.
109 A. T. Biju, N. Kuhl and F. Glorius, *Acc. Chem. Res.*, 2011, **44**,

1182–1195.

This journal is © The Royal Society of Chemistry 20xx

Suggested Text for the Table of Contents Entry

This Feature Article offers in-depth, design-to-application discussions of redox-switchable N-heterocyclic carbenes that have been field tested.

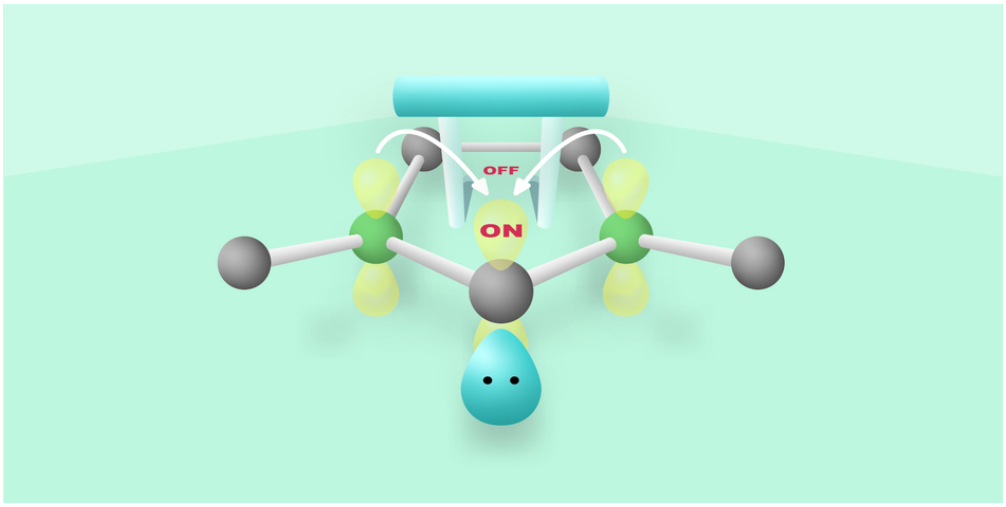

80x39mm (300 x 300 DPI)